Journal of Molecular Liquids 352 (2022) 118754

Contents lists available at ScienceDirect

Journal of Molecular Liquids

journal homepage: www.elsevier.com/locate/molliq

L-menthol-based eutectic solvents: Characterization and application in the removal of drugs from water

Fernando Bergua [a,c], Miguel Castro [b,d], José Muñoz-Embid [a,c], Carlos Lafuente [a,c], Manuela Artal [a,c,*]

[a] Departamento de Química Física, Facultad de Ciencias, Universidad de Zaragoza, Zaragoza, Spain
[b] Departamento de Ciencia y Tecnología de Materiales y Fluidos, Universidad de Zaragoza, Zaragoza, Spain
[c] Instituto Agroalimentario de Aragón – IA2 (Universidad de Zaragoza – CITA), Zaragoza, Spain
[d] Instituto de Nanociencia y Materiales de Aragón (INMA) Universidad de Zaragoza – CSIC, Zaragoza, Spain

ARTICLE INFO

Article history:
Received 12 November 2021
Revised 8 February 2022
Accepted 11 February 2022
Available online 15 February 2022

Keywords:
L-menthol
Carboxylic acid
Eutectic
Emerging contaminants
Thermophysical properties
Solubility and extraction

ABSTRACT

Increasing the sustainability of industrial processes implies the substitution of conventional solvents for others with less environmental impact. For its implementation, it is essential to know the value of the thermodynamic and transport properties. In addition, having theories and correlations to predict their behaviour under varied conditions is very interesting. In this work, we performed the thermophysical characterization of eutectic mixtures formed by L-menthol and medium chain fatty acids, deepening the study of the polymorphic behaviour of L-menthol. In addition, we studied their ability both to dissolve drugs that are poorly soluble in water and to extract them from contaminated water. From the results, we can deduce that these mixtures may be suitable solvents in liquid-liquid extractions, although multistage processes can be necessary.

1. Introduction

The implementation of solvent-free processes would be ideal to reduce their environmental impact but unrealistic since their presence is essential both for the dissolution, suspension or extraction of compounds and to facilitate the transfer of mass and heat. The Petrochemical Group European estimates that the organic solvents industry in Europe directly employs approximately 10,000 people and indirectly employs more than 10 million people, with a turnover of the producing enterprises of close to €5 billion [1]. For 2023, the global market for these compounds is expected to exceed €40 billion with a demanded volume higher than 24,500 kilotons. More than half of the consumption is attributed to the paint and coating and pharmaceutical industries [2]. Despite the above, the increase in environmental awareness has led to the approval of regulations such as the Registration, Evaluation and Authorization of Chemicals (REACH) aimed at limiting the use of these compounds by replacement with other more benign compounds. Increasing sustainability in industries includes studying the problems derived from the use of conventional solvents. The solutions can go through the drastic modification of the processes or at least the increase of its efficiency or the recycling of the solvent to minimize its consumption. Another possibility is conventional solvent replacement by another, pure or mixture, with similar behaviour but lower toxicity, so the cost of implementation would be low. For this purpose, different companies and organizations have developed a selection of computer tools. In 2016, Byrne et al. [3] published a review analysing several guides proposed mostly by the pharmaceutical industry. These guides explained the differences and similarities between them and highlighted the lack of transparency in the methodology used to choose the alternative solvent. They concluded that knowledge regarding the physical properties and environmental impact of neoteric solvents should be expanded by stimulating the design of new mixtures. Other more recent tools are the program for assisting the replacement of industrial solvents (PARIS III) [4] developed by the Environmental Protection Agency and sustainable solvent selection and substitution software (SUSSOL) [5] based on artificial intelligence. All of these tools require a database of thermophysical properties, such as density, phase equilibrium, refractive index, surface tension, heat capacity, viscosity, Hansen's parameters, solubility in water or partition coefficients. These values can be both experimental data taken from the literature and calculated from thermodynamic models or equations of state that must be previously validated. In addition, the newer tools also include criteria related to environmental impact. The review published by Clark et al. [6] contains

* Corresponding author at: Departamento de Química Física, Facultad de Ciencias, Universidad de Zaragoza, Zaragoza, Spain.
E-mail address: martal@unizar.es (M. Artal).

https://doi.org/10.1016/j.molliq.2022.118754
0167-7322/

an exhaustive analysis of technical, economic and environmental issues of the most promising alternative solvents: renewable solvents, ionic liquids, liquid polymers, CO_2-based solvents, and deep eutectic solvents (DESs). Both the choice of one type or another neoteric solvent and the total or partial substitution of the conventional solvent will depend on many factors. DESs can be defined as mixtures in which the fusion properties of the components, the interactions between them, and the entropic effect in the mixing process cause a decrease in the melting temperature with respect to the melting temperature of the ideal system. For some systems, this decrease $(\Delta T_m = T_{m,\mathrm{exp}} - T_{m,\mathrm{id}})$ is very pronounced. Five categories have been proposed depending on the nature of the compounds in the mixture [7]. Three of these categories (types I, II, and IV) contain metal salts and therefore are less attractive from an environmental point of view. Conversely, type III CsMPs are composed of organic salts and metabolites, so they are often called natural eutectics (NADESs) [8]. Finally, type V DESs are ionic and nonionic eutectic mixtures with high hydrophobic character. The interactions between their components are weaker than in the previous types, so ΔT_m can be very small. Thus, we prefer the term eutectic solvents (ESs) to refer to them. For every DES, types III and V are easy and do not require waste generation procedures, but most DESs have high biodegradability and low toxicity, so they can be classified as green solvents. Literature reviews about the great possibilities of hydrophilic and hydrophobic NADESs for biotechnological applications have been published [9,10]. In pharmacology, low solubility implies increasing the dose that must be administered to reach the desired plasma level, which can cause problems related to an increase in the side effects of the drug, especially if a combination of several active principles is necessary. NADESs are being researched as drug vehicles of poorly soluble active principles in aqueous media, including so-called multidrug eutectics, since these substances can become much more soluble in these eutectics [11–15]. The final formulation in the liquid phase will be especially suitable for parenteral administration and in patients with swallowing problems. Other applications, more specific to hydrophobic ESs, are gas solubilization, formation of membranes, hydrogels and ferrofluids, and removal of contaminants from aqueous media [15–20]. The latter application is growing in importance in light of the estimated figures for water demand in the future. According to the United Nations World Water Development Report (2018) [21], water use has increased sixfold in the last 100 years and is expected to reach 6,000 km^3/year by 2050. In addition, a quality problem should be added. An estimated 80% of all wastewater is released to the environment without prior treatment. In some countries, up to 200 different drugs have been detected in the effluents [22,23], and their effect on health should not be underestimated even if the concentration is low. These compounds have a wide variety of physicochemical properties, current treatments have shown partial effectiveness [24], and other procedures should be evaluated. Liquid-liquid extraction with hydrophobic ESs is a suitable technique. In the literature, we have found studies about the removal of phenolic compounds, boron, and drugs from water using this procedure [15,25–28]. Specifically, the systems studied in this work, L-menthol + octanoic acid ([Men:Oct]) or L-menthol + decanoic acid ([Men:Dec]) have shown promising results as extraction media of organic compounds and metals from wastewater [29–35]. Rodriguez-Llorente al. [36] have shown that several pure terpenes can be good solvents in extraction processes. This possibility has been not evaluated here due to the melting point of L-menthol is above the room temperature. For temperatures near 318 K, literature reports thermal degradation both quercetin and tetracycline, especially if the temperature is maintained several hours [37,38].

To optimize these processes in the industry, it is necessary to know the temperature range for which the solvents are liquids as well as the values of different thermodynamic and transport properties and the effect of the temperature on the solvents. Nevertheless, studies including their characterization are scarce. Several authors have determined different thermophysical properties [25,34,47–49,39–46], but some papers did not provide numerical values. Theoretical studies about their structure and stability have also been published [50,51].

The first aim of this work was to characterize eutectic mixtures composed of L-menthol and two carboxylic (octanoic and decanoic) acids to be proposed as alternative solvents in different fields. L-menthol was chosen because is the main form of menthol in nature. Furthermore, the racemic mixture showed additional anomalies in a preliminary thermal characterization. To tackle the goal, we studied the solid-liquid equilibria of both systems, including the effect of the polymorphic behaviour of L-menthol. In addition, we determined several thermophysical properties, such as density, speed of sound, isobaric molar heat capacity, refraction index, static permittivity, surface tension, and viscosity. From these values, we calculated derived properties and validated several correlations and thermodynamic models. The second purpose was to explore the ability of these liquids to dissolve poorly soluble compounds in an aqueous medium. For that purpose, we measured the solubility of quercetin, nitrofurantoin and tetracycline in the [Men]ESs previously characterized and evaluated their efficacy in extracting these drugs from contaminated water.

2. Material and methods

2.1. Chemicals

Compounds used to prepare the eutectic solvents (ESs) were L-menthol (Men), octanoic acid (Oct), and decanoic acid (Dec), and the active principles used in the solubilization and extraction study were quercetin (Q), nitrofurantoin (NF) and tetracycline (TC). They were supplied by Sigma–Aldrich (Germany) and used as received. The characteristics and structure of these compounds are reported in Table 1 and Fig. 1. The studied systems were prepared by mixing Men and Oct or Dec at moderate temperature (323 K) with stirring until a homogeneous liquid was formed. The components were weighed with a PB210S Sartorius balance ($u(m) = 1{\cdot}10^{-4}$g) in molar ratios of 1:2, 1:1, and 2:1. The characteristics of the L-menthol-based ESs ([Men]ESs), including the acronym, the composition, the calculated molar mass (M) and the measured melting temperature (T_m), are listed in Table 2. The pH of the mixtures ranged from 4.0 to 4.5.

2.2. Calorimetric characterization

The solid-liquid equilibria (SLE) were determined with a differential scanning calorimeter (TA Instruments DSC Q2000) with an RCS cooling system. Temperature and heat flow calibrations were performed using the melting transition of indium as a standard sample. The differences with the expected values showed that the uncertainties in T_m and $\Delta_m H$ were 0.5 K and 1%, respectively. For each mixture, a sample (5–15 mg) was weighed and introduced into an aluminium pan in the liquid state. If the sample was solid at room temperature, a preheating step in the DSC up to a temperature higher than the liquidus was performed to ensure crystallization within the device. The samples were initially cooled to 203–213 K at 3 K/min and later heated at the same scanning rate up to 10 K above the phase change. The reported temperatures correspond to the maximum peak temperature because several thermal anomalies made it difficult to determine the onset temperature.

Table 1
Relevant properties of compounds used in this work. Molar mass (M), melting temperature (T_m), melting enthalpy ($\Delta_m H$), dipole moment (μ), and polarizability (α).

Chemical (Acronym)	Purity[a]	M/g·mol^{-1}	T_m/K	$\Delta_m H$/kJ·mol^{-1}	μ/D	α/Å^3
L-menthol (Men)	>0.99	156.27	315.2 ± 0.5[b] 316.4 ± 0.9[52]	13.1 ± 0.1[b] 12.9 ± 1.3[52]	1.57[53]	
Octanoic acid (Oct)	>0.99	144.21	288.4 ± 0.5 [15]	20.2 ± 0.2 [15]	1.15[53]	
Decanoic acid (Dec)	>0.98	172.26	304.4 ± 0.5 [15]	27.7 ± 0.3 [15]	–	
Quercetin (Q)	>0.95	302.24	589.6[54]	–	2.8522[55]	34.67[55]
Nitrofurantoin (NF)	>0.98	238.16	536[54]	–	4.91[56]	19.85[56]
Tetracycline (TC)	>0.95	444.43	445.6[54]	–	6.11[56]	40.92[56]

[a] As stated by the supplier by Sigma–Aldrich (mass fraction).
[b] This work.

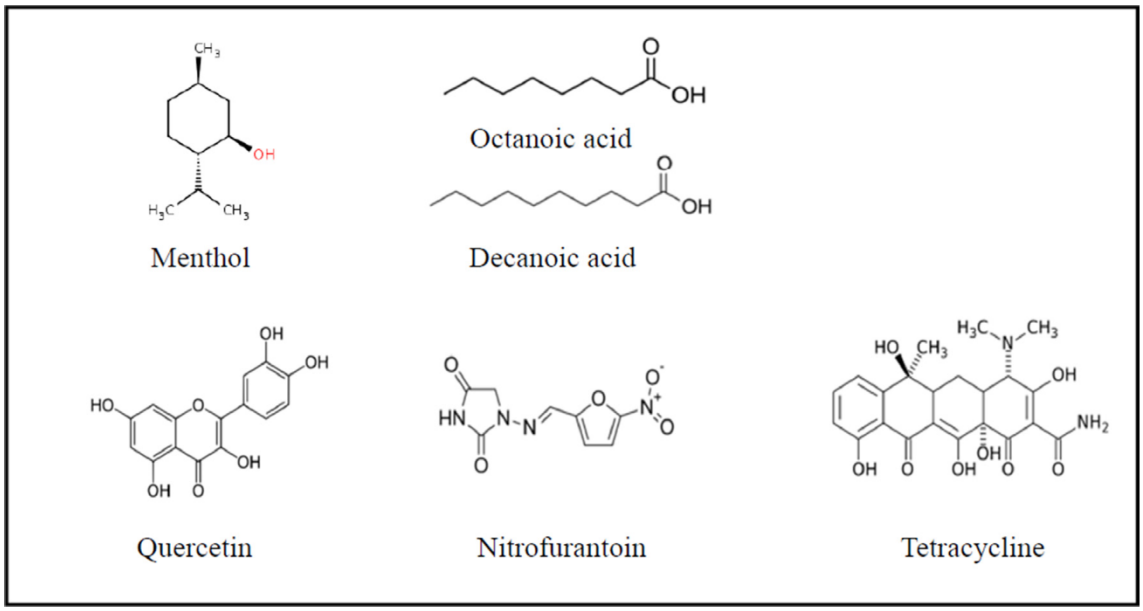

Fig. 1. Structure of the compounds used in this study.

Table 2
Characteristics of L-menthol-based eutectic mixtures studied in this work.

Acronym	Component 1	Component 2	Molarratio	M[a]/g·mol^{-1}	T_m/K	p_v[c]/Pa
[Men:Oct] (1:2)	L-menthol	Octanoic acid	1:2	148.23	276.1[b]	3.33
[Men:Oct] (1:1)	L-menthol	Octanoic acid	1:1	150.24	262.8[b]/268.65[49]	5.07
[Men:Oct] (2:1)	L-menthol	Octanoic acid	2:1	152.25	282.0[b]	6.90
[Men:Dec] (1:2)	L-menthol	Decanoic acid	1:2	166.93	284.8[b]	3.31
[Men:Dec] (1:1)	L-menthol	Decanoic acid	1:1	164.26	287.5[b]/286.20[49]	5.08
[Men:Dec] (2:1)	L-menthol	Decanoic acid	2:1	161.60	292.8[b]	6.89

[a] $M = \sum_i M_i x_i$.
[b] This work; $u(T_m) = 0.5$ K.
[c] PC-SAFT Predicted values, $T = 298.15$ K.

Additionally, sapphire was used as the recommended standard material to obtain the isobaric molar heat capacity values. Two sapphire experiments were carried out before and after each daily measurement session to discard any temporal evolution of the heat capacity calibration factor. The uncertainty in $C_{p,m}$, calculated by comparison with the accepted values in the 263–343 K temperature range, was lower than 1%.

2.3. Thermophysical characterization

Properties such as density (ρ), speed of sound (u), refraction index (n_D), static permittivity (ε), surface tension (γ), and kinematic viscosity (ν) were measured with several thermostatically controlled devices, summarized in Table S1 (Supplementary Material), and no full description was made because these techniques are commonly reported in the bibliography. The equipment was tested [13,57] by comparing the values of the experimental properties of benzene (>99.5% purity) with the properties from the literature. For each apparatus, Table S1 summarizes the standard uncertainty in the temperature ($u(T)$), the calculated combined expanded uncertainties for each property ($U_c(Y)$), and the mean relative deviations ($MRD(Y)$) obtained from the check.

2.4. Solubility and extraction experiments

The shake-flask method was used to measure the solubility (W) of the Q, NF, and TC in [Men]ESs. The solute was added to each eutectic solvent until supersaturation, and the flask was placed at

a constant temperature of 298.15 K, in an ultrasound bath to ensure correct mixing. After resting, centrifugation and filtration (PES syringe filter, 0.22 μm), three samples were taken for analysis by UV–VIS spectroscopy with a double-beam spectrum VWR 6300 PC ($u(\lambda)$ = ±0.2 nm). The calibration curves with the detection and quantification limits are listed in Table S2. The experiment was repeated three times, so the solubility value for each drug was the average of nine analyses. To carry out the extraction study, aqueous solutions of Q, NF, or TC were prepared. The concentrations measured by UV–VIS were C_i(Q) = 0.5 μM, C_i(NF)= 30 μM, and C_i(TC) = 70 μM. Similar volumes of each solution and [Men] ESs were mixed, and the aqueous phase was collected, treated, and analysed as described above. The composition measured (C_f) allowed us to calculate the extraction efficiency as $EE = 100(C_i - C_f/C_i)$.

3. Results and discussion

3.1. Solid-liquid equilibria

In this section, a detailed thermal study of L-menthol + octanoic acid ([Men:Oct]) and L-menthol + decanoic acid ([Men:Dec]) is reported. For each component, the temperature and enthalpy of fusion from our measurements and the selected data from the literature [58–61] are listed in Table 1. The values matched considering the experimental uncertainties. L-Menthol is known to present complicated polymorphic behaviour with several possible crystalline phases [58–60]. To date, up to four different phases ($\alpha, \beta, \gamma, \delta$) have been found [59]. The first phase is the stable phase, and the reported data in Table 1 refer to it; the other three phases are metastable phases. Using conventional DSC, concomitant polymorphisms were detected [59,62]. That is, simultaneous crystallization of the four phases occurred with an instant conversion of the metastable phases to a more stable phase. From the literature [59–61,63], it can be deduced that the time-thermal history experienced by the sample will govern the presence and possible detection of the different phases. To check how this fact can affect our measurements, we performed a thermal study of pure L-menthol at different cooling rates: 3, 10, 15, 20 and 30 K/min. In all cases, a subsequent heating process at 3 K/min was applied. The thermograms are displayed in the Supplementary Material (Fig. S1). At the lowest rate (3 K/min), only a single melting peak was detected at T_m = 314.90 K and $\Delta_m H$ = 12.90 kJ/mol, in agreement with the reported data of the α phase (Table S3). When the cooling rate increased, the heating thermogram revealed two peaks. The lowest peak, at T_m = 309.44 K and $\Delta_m H$ = 12.26 kJ/mol, agreed with the values of the metastable β-phase (Table S3). We estimated the percentage of each phase in all samples from the mean enthalpy content and our experimental values (Table S4). No indication of the two other metastable phases was obtained. Therefore, a scanning rate of 3 K/min could be the best election to assure the presence of only the stable phase of pure L-menthol. Nevertheless, we must consider that its crystallization behaviour could be different in the mixtures [58]. To apply these solvents in the industry, it is essential to determine their liquid-solid phase diagrams (SLEs) since they show the compositions for which the system is liquid.

Additionally, the comparison of the real melting temperature with the ideal melting temperature provides information about the interactions between the components. All the heating thermograms (Fig. 2) showed multiple endothermic peaks related to the presence of eutectic and liquidus fractions. The liquidus peak presented a pretail, typical of these systems, [64] covering a temperature interval dependent on the composition. In mixtures near the eutectic composition, four and three thermal anomalies were observed for [Men:Oct] and [Men:Dec], respectively. This phenomenology contrasts with the SLE data already published where only one or two eutectic phases were reported [49,58], possibly due to our experimental procedure, as we use lower cooling and heating rates. The number of eutectic peaks increased with the acid mole fraction, although some of them were only small shoulders. Similar mixtures based on menthol and fatty acids with a higher aliphatic chain, such as stearic acid, myristic acid and lauric acid, showed comparable behaviour [65]. The existence of more than one eutectic peak was related to the complex polymorphism of L-menthol. Therefore, the addition of the acid component seems to favour the appearance of metastable phases and the formation of the corresponding eutectic mixture. Furthermore, a careful examination of Fig. 2 revealed small exothermic peaks close to the eutectic temperature for both systems in the Men-rich region. None of these events was found at acid-rich compositions. Moreover, these events occurred at approximately 268 K, at which the highest β-α transformation rate of pure L-menthol has been reported [59,60]. Therefore, the events could be due to the recrystallization of the L-menthol present in the metastable eutectic fraction. We can conclude that the peak with the highest temperature corresponds to the eutectic involving the stable phase (α) and the other peaks correspond to the metastable phases.

Table S5 lists the experimental melting temperatures for our systems. The values were correlated with the nonrandom two-liquid (NRTL) model [66] (Supplementary Material), and the coefficients are reported in Table 3. Fig. 3 displays the experimental and correlated values and those published by Martins et al. [49] that were in a good agreement with ours. The eutectic compositions can be obtained with Tamman diagrams using the melting enthalpies of the mixtures. Due to the complexity of our thermograms, calculations with deconvolutions were required. The procedure and equations are shown in the Supplementary Material, and the parameters are listed in Table S6. An example of the deconvolution for each system is shown in Fig. 4. The representations include the peak corresponding to the melting of the liquidus fraction extracted from the deconvolution and the total fitting curve as the sum of the three peaks. These latter nicely follow the experimental data. With the above, the estimated eutectic points were x^E_{Men} = 0.533, T^E_{m} = 263.8 K for the [Men:Oct], and x^E_{Men} = 0.615, T^E_{m}=289.9 K for the [Men:Dec].

The classical thermodynamic allows us to calculate the solubility of the solid in the liquid phase for systems totally miscible in the liquid phase and immiscible in the solid phase as follows:[67]

$$\ln\left(x_i\gamma_i^l\right) = \frac{\Delta_m H_{m,i}}{R}\left(\frac{1}{T_{m,i}} - \frac{1}{T_m}\right) + \frac{\Delta_m C_{p,i}}{R}\left(\frac{T_{m,i}}{T_m} - \ln\frac{T_{m,i}}{T_m} - 1\right) \qquad (1)$$

where γ_i^l, $T_{m,i}$, $\Delta_m H_i$, and $\Delta_m C_{p,i}$ are the following properties of component i: the activity coefficient in the liquid phase at composition x_i, the melting temperature (K), the melting enthalpy (J·mol^{-1}), and the variation in the heat capacity in the liquid and solid phases. Moreover, T_m is the melting temperature (K) of the mixture. The second term in Eq. (1) is negligible since its value is usually much less than the value for the first. If ideal behaviour is assumed, the phase equilibrium is easily obtained since γ_i^l = 1. Both studied systems showed a slight negative deviation from ideality that was more pronounced for the Men-rich compositions (Fig. 3). For non-ideal calculations, several thermodynamic models can be used to obtain the activity coefficients and subsequently the liquidus lines. We have chosen the PC-SAFT equation of state (EoS) [68,69] to predict the fugacity coefficients of component i in the mixture (φ_i) and in the pure state (φ_i^0) since $\gamma_i^l = \varphi_i/\varphi_i^0$. This model is widely validated in the literature and is summarized in the Supplementary Material. Table S7 lists the parameters for the pure compounds. The model provided a good representation of the phase equilibria

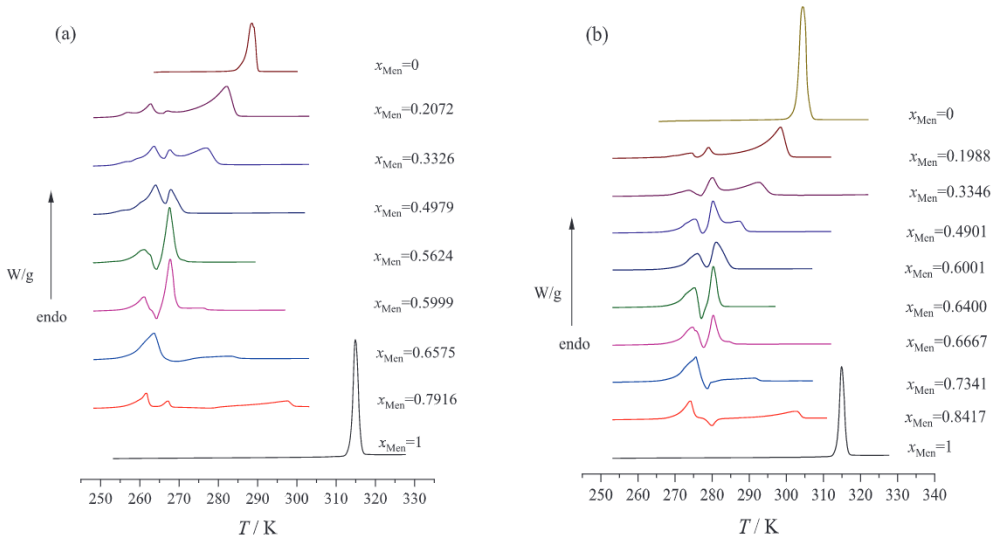

Fig. 2. Thermograms of L-menthol-based ESs: (a) [Men:Oct]; (b) [Men:Dec].

Table 3
NRTL correlation parameters and deviations in the melting temperature of the [Men]ES systems.

System	A_{12} /J·mol^{-1}	A_{21} /J·mol^{-1}	$AAD(T_m)$[a]/K	$MRD(T_m)$[b]/%
[Men:Oct]	2720.53	−3486.89	0.9	0.33
[Men:Dec]	2407.11	−2905.92	1.3	0.45

[a] $AAD(Y) = \frac{1}{n}\sum_{i=1}^{n}\left|Y_{i,calc} - Y_{i,exp}\right|$.
[b] $MRD(Y) = \frac{100}{n}\sum_{i=1}^{n}\left|\frac{Y_{i,calc}-Y_{i,exp}}{Y_{i,exp}}\right|$.

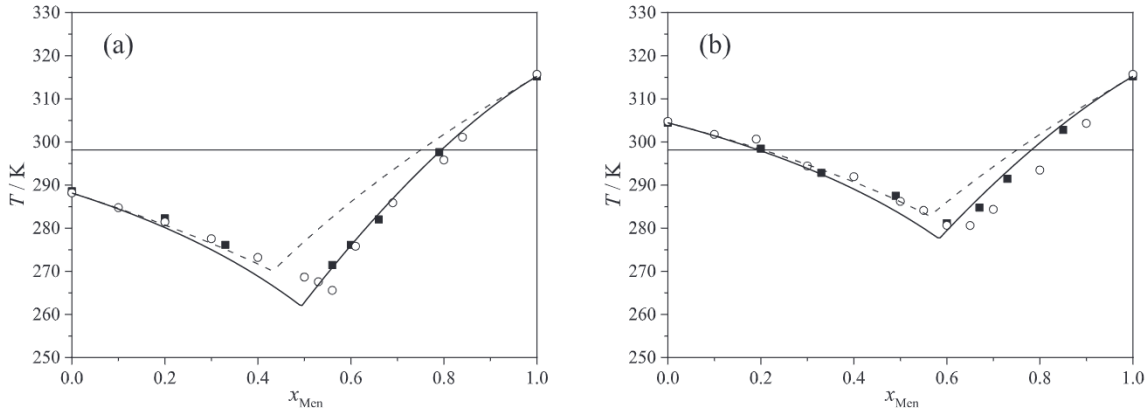

Fig. 3. Solid-liquid equilibria of L-menthol-based ESs: (a) [Men:Oct]; (b) [Men:Dec]. (■), this work; (○), Ref. [49]; (----), Ideal; (____), NRTL.

(Tables S5, S8) with mean relative deviations, $RMD(T_m)$, between experimental and predicted values from 0.07 to 2.5%.

3.2. Thermophysical study

The use of new solvents in the industry requires prior knowledge of their thermodynamic and transport properties as well as the effect of temperature on them. In this section, the values of seven properties of [Men]ESs as a function of the temperature (T) and at $p = 0.1$ MPa are presented and discussed. The studied mixtures were L-menthol + octanoic ([Men:Oct]) and decanoic acid ([Men:Dec]) in molar ratios of 1:2, 1:1 and 2:1. The lower working temperature varied for each ES depending on their melting point, and the upper working temperature was always 338.15 K. The measured properties were the density (ρ), speed of sound (u), isobaric molar heat capacity ($C_{p,m}$), refraction index (n_D), static permittivity (ε), surface tension (γ), and kinematic viscosity (ν). Tables S9 and S10 list their values at each temperature and composition, and Table 4 summarizes those values for $T = 298.15$ K to ease the following of the text.

However, since the operational conditions do not always match the conditions used in the characterization, having correlations and models that allow predicting the values is highly advisable. The relationship between most of the thermodynamic properties and the temperature is linear, and that for the transport properties

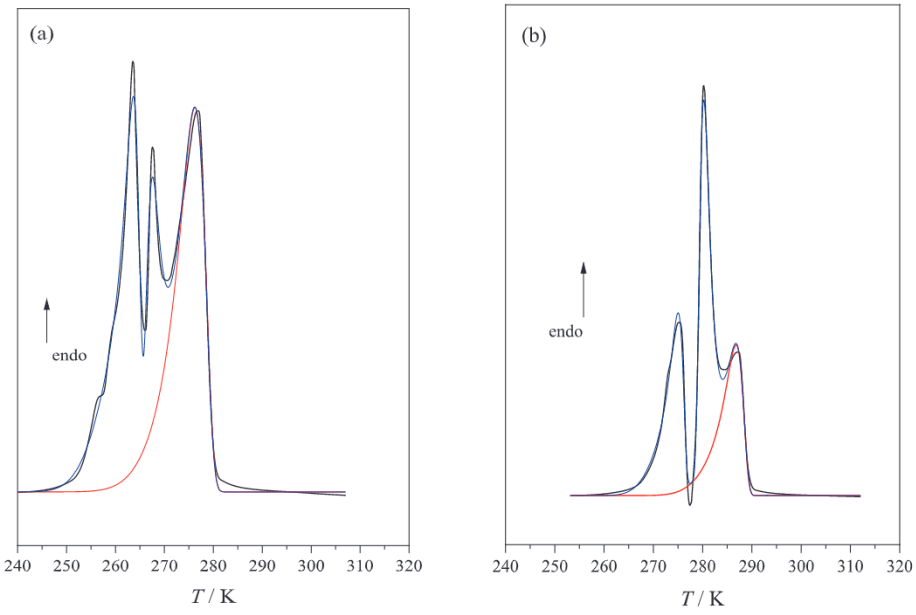

Fig. 4. Deconvolutions for (a) [Men:Oct], x_{Men} = 0.3330; (b) [Men:Dec], x_{Men} = 0.4910 (—), experimental curve; (—), experimental fitting; (—), liquidus fitting.

Table 4
Summary of the experimental and calculated thermophysical properties at T = 298.15 K and p = 0.1 MPa of the studied [Men]ESs mixtures.

	[Men:Oct]			[Men:Dec]		
Property	(1:2)	(1:1)	(2:1)	(1:2)	(1:1)	(2:1)
ρ/kg·m^{-3}	902.88	901.09	899.35	896.15	896.06	895.94
u/m·s^{-1}	1325.57	1334.85	1343.79	1348.46	1352.34	1355.66
$C_{p,m}$/J·mol^{-1}·K^{-1}	299	313	298	351	343	349
n_D	1.43849	1.44396	1.44946	1.44227	1.44651	1.45079
ε	3.286	3.885	4.201	3.068	3.451	3.845
γ/mN·m^{-1}	28.32	28.29	28.30	29.07	28.79	28.47
η/mPa·s	8.809	12.046	17.598	12.757	15.814	21.116
α_p/kK^{-1}	0.850	0.839	0.833	0.834	0.826	0.823
κ_s/TPa^{-1}	630.33	622.83	615.76	613.68	610.23	607.32
L_f/Å	0.496	0.493	0.490	0.490	0.488	0.487
R_m/cm^3·mol^{-1}	43.139	44.285	45.447	49.313	48.932	48.546
f_m/cm^3·mol^{-1}	121.04	122.45	123.84	136.96	134.38	131.82
$g\mu^2$/D^2	1.55	2.23	2.58	1.45	1.89	2.32
ΔS_S/mN·m^{-1}·K^{-1}	0.077	0.074	0.077	0.077	0.076	0.074
ΔH_S/mN·m^{-1}	51.23	50.33	51.28	52.03	51.48	50.50
$E_{a,\eta}$/kJ·mol^{-1}	28.2	32.9	40.4	30.7	34.4	41.2

Standard uncertainties are: $u(T)$ = 0.005 K for density and speed of sound and 0.01 K for the rest of properties; $u(p)$ = 0.5 kPa. The combined expanded uncertainties (0.95 level of confidence, k = 2) are$U_c(\rho)$ = 0.05 kg·m^{-3}; $U_c(u)$ = 0.5 m·s^{-1}; $U_c(C_{p,m})$ = 1%; $U_c(n_D)$ = 2·10^{-5}; $U_c(\varepsilon)$ = 1%; $U_c(\gamma)$ = 1%; $U_c(\eta)$ = 1%; $U_c(\alpha_p)$ = 0.04 kK^{-1}; $U_c(\kappa_s)$ = 0.24 TPa^{-1}; $U_c(L_f)$ = 0.005 Å; $U_c(R_m)$ = 0.004 cm^3·mol^{-1}; $U_c(f_m)$ = 0.03 cm^3·mol^{-1}; $U_c(\Delta S_S)$ = 0.001 mN·m^{-1}·K^{-1}; $U_c(\Delta H_S)$ = 0.06 mN·m^{-1}; $U_c(E_{a,\eta})$ = 0.10 kJ·mol^{-1}.

is exponential. We correlated the $\rho, u, C_{p,m}, n_D$, and γ experimental data with a linear equation, the ε for some mixtures with a second-degree polynomial, and the dynamic viscosity ($\eta = \rho\nu$) with a VFT expression. Table 5 lists the equations and the fit parameters.

The density of the studied [Men]ESs ranged from 866 to 916 (±0.05) kg.m^{-3}. These values were 8.5% lower than those of water, so these solvents can be used in processes of phase separation [47]. The mixtures containing Oct were slightly denser than those with Dec due to the larger size of the latter. In both systems, ρ decreased with increasing L-menthol molar ratio (x_{Men}), but for [Men:Dec], this change was indiscernible. In fact, considering the experimental uncertainty in the density measurement, these mixtures can hardly be considered distinguishable. As expected, the thermal motion decreased the density, as shown in Fig. 5a. We quantified the effect of the temperature on the density by calculating the isobaric thermal expansibility ($\alpha_p = -(\partial \ln \rho/\partial T)_p$). The values obtained (Fig. 6a) decreased with increasing hydrocarbon chains as well as x_{Men}. However, increasing the temperature increased the expansion capacity of the fluids.

In the literature, we found some papers containing ρ data of these mixtures at similar temperatures. Nunes et al. [45] published densities for the [Men:Oct] system at the three compositions. Adeyemi et al. [40] studied both systems at the (1:2) molar ratio. Sas et al. [25] and Gonzalez et al. [39] reported data for both equimolar mixtures. Van Osch et al. [47] measured densities of [Men:Dec] systems at 298.15 K and at the compositions (1:1) and (2:1). Our values were in agreement with all of them, and the average mean relative deviations were $\overline{MRD}(\rho)$ = 0.45, 1.12, 0.07, 0.03, and 0.40%. A graphical comparison is shown in Fig. S2a.

The speed of sound values of Men[ESs] ranged from 1184 to 1405 m·s^{-1} (Fig. S3a). From the ρ and u data, we estimated the

Table 5
Fit parameters (A_Y, B_Y, C_Y) and the regression coefficients, R^2, for the thermophysical properties of the studied [Men]ESs.

Property	[Men]ESs	A_Y	B_Y	C_Y	R^2
ρ[a]/kg·m^{-3}	[Men:Oct] (1:2)	1131.60	−0.7671		0.99999
	[Men:Oct] (1:1)	1126.51	−0.7562		0.99997
	[Men:Oct] (2:1)	1122.62	−0.7489		0.99996
	[Men:Dec] (1:2)	1118.93	−0.7472		1.0000
	[Men:Dec] (1:1)	1116.80	−0.7403		1.0000
	[Men:Dec] (2:1)	1115.73	−0.7372		0.99997
u[a]/m·s^{-1}	[Men:Oct] (1:2)	2374.45	−3.5180		0.99977
	[Men:Oct] (1:1)	2378.74	−3.5009		0.99998
	[Men:Oct] (2:1)	2384.34	−3.4905		0.99992
	[Men:Dec] (1:2)	2353.39	−3.3729		0.99972
	[Men:Dec] (1:1)	2356.83	−3.3698		0.99979
	[Men:Dec] (2:1)	2356.26	−3.3561		0.99978
$C_{p,m}$[a]/J·mol^{-1}·K^{-1}	[Men:Oct] (1:2)	105.125	0.64955		0.99984
	[Men:Oct] (1:1)	38.266	0.92277		0.99993
	[Men:Oct] (2:1)	38.189	0.87282		0.99992
	[Men:Dec] (1:2)	200.975	0.50287		0.99952
	[Men:Dec] (1:1)	125.358	0.73071		0.99981
	[Men:Dec] (2:1)	77.556	0.91012		0.99991
n_D[a]	[Men:Oct] (1:2)	1.55818	$-4.01\cdot10^{-4}$		0.99999
	[Men:Oct] (1:1)	1.56385	$-4.02\cdot10^{-4}$		0.99998
	[Men:Oct] (2:1)	1.56958	$-4.03\cdot10^{-4}$		0.99996
	[Men:Dec] (1:2)	1.56029	$-3.96\cdot10^{-4}$		1.0000
	[Men:Dec] (1:1)	1.56436	$-3.95\cdot10^{-4}$		0.99999
	[Men:Dec] (2:1)	1.57030	$-4.01\cdot10^{-4}$		0.99997
ε[b]	[Men:Oct] (1:2)	4.184	−0.0030		0.9849
	[Men:Oct] (1:1)	11.59	−0.042	$5.42\cdot10^{-5}$	1.000
	[Men:Oct] (2:1)	20.70	−0.096	$1.36\cdot10^{-4}$	1.000
	[Men:Dec] (1:2)	3.735	−0.0023		0.9806
	[Men:Dec] (1:1)	4.860	−0.0047		0.9966
	[Men:Dec] (2:1)	15.56	−0.0664	$9.08\cdot10^{-5}$	1.000
γ[a]/mN·m^{-1}	[Men:Oct] (1:2)	51.12	−0.077		0.99971
	[Men:Oct] (1:1)	50.34	−0.074		0.99979
	[Men:Oct] (2:1)	51.21	−0.077		0.99986
	[Men:Dec] (1:2)	52.04	−0.077		0.99976
	[Men:Dec] (1:1)	51.67	−0.076		0.99960
	[Men:Dec] (2:1)	50.56	−0.074		0.99931
η[c]/mPa·s	[Men:Oct] (1:2)	0.01339	1106.02	127.79	0.99995
	[Men:Oct] (1:1)	0.03008	804.02	163.77	0.99998
	[Men:Oct] (2:1)	0.02793	760.19	180.25	1.0000
	[Men:Dec] (1:2)	0.03728	847.74	155.37	1.0000
	[Men:Dec] (1:1)	0.03090	836.20	164.11	1.0000
	[Men:Dec] (2:1)	0.02479	817.05	177.05	0.99999

[a] $Y = A_Y + B_Y T$.
[b] $Y = A_Y + B_Y T + C_Y T^2$.
[c] $Y = A_Y \exp[B_Y/(T - C_Y)]$;$A_\eta$/mPa·s = η_∞.

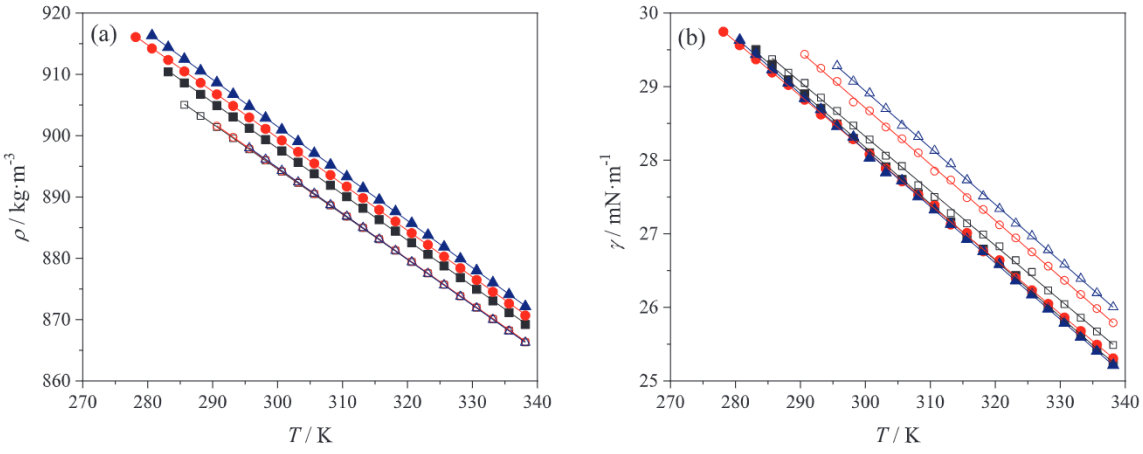

Fig. 5. Experimental thermodynamic properties of [Men]ESs at several temperatures, T, and compositions: (▲), (1:2); (●), (1:1); (■), (2:1) in molar ratio. (a), Density, ρ; (b), surface tension, γ. Full symbols, [Men:Oct]; open symbols, [Men:Dec]. Lines, correlated data.

packing of the fluids by calculating the intermolecular free length (L_f) related to the isentropic compressibility ($\kappa_S = 1/\rho u^2$) as follows: $L_f = K\sqrt{\kappa_S}$, where K is Jacobson's constant [70]. The calculated κ_S and L_f values decreased with increasing x_{Men} and chain length and increased with thermal motion (Table 4, Fig. 6b). Sas et al. [25] have reported u data of the equimolar mixtures of both

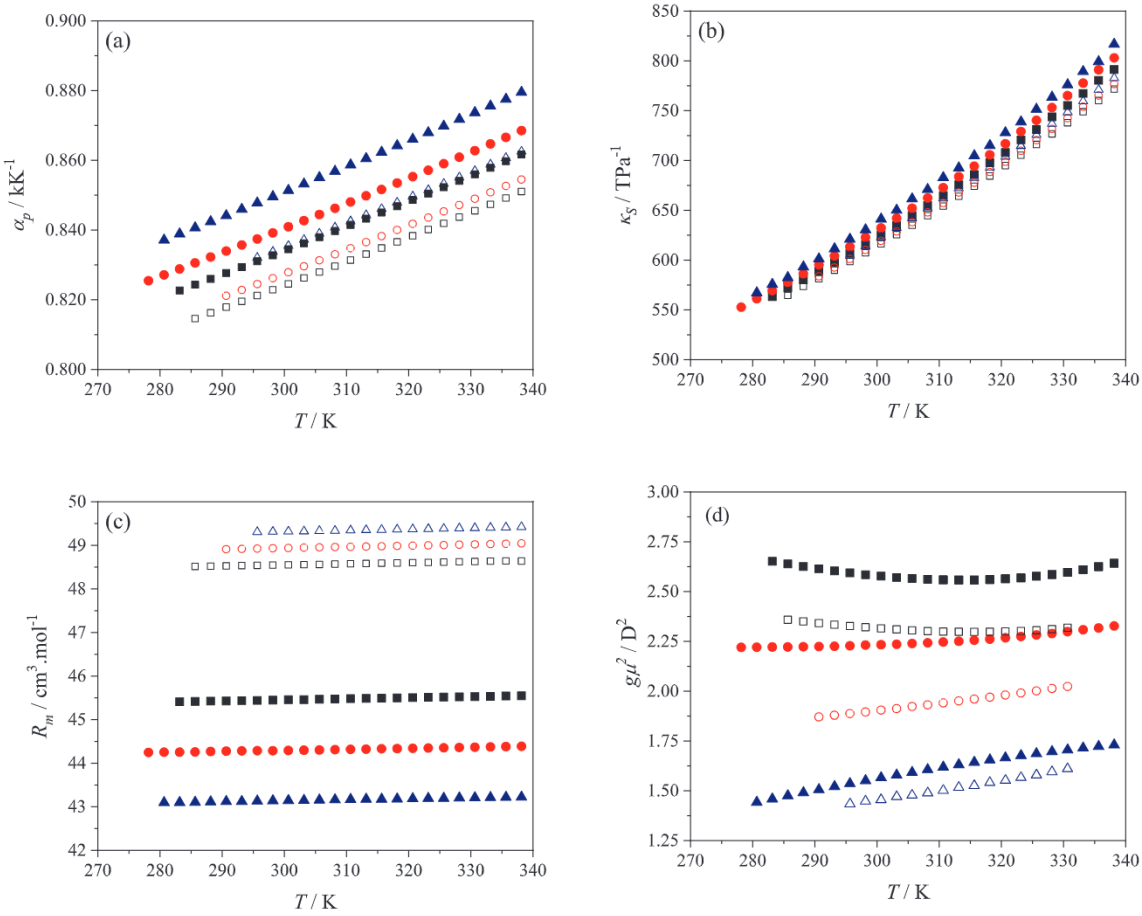

Fig. 6. Calculated thermodynamic properties of [Men]ESs at several temperatures, T, and compositions: (▲), (1:2); (●), (1:1); (■), (2:1) in molar ratio. (a) Isobaric thermal expansibility, α_p; (b) isentropic compressibility, κ_s; (c) molar refraction, R_m; (d), orientational dipolar parameter, $g\mu^2$. Full symbols, [Men:Oct]; open symbols, [Men:Dec].

systems. Fig. S1b shows the graphical comparison, and the average deviation was $\overline{MRD}(u) = 0.25\%$.

The isobaric molar heat capacity of the [Men]ESs ranged from 285 to 386 J·mol^{-1}·K^{-1}. The values for the [Men:Dec] mixtures were higher than for [Men:Oct] with an average difference of 44 J·mol^{-1}·K^{-1} at 298.15 K. This property is a function of temperature and molar mass. For both systems, $C_{p,m}$ increased linearly with T, but the slope in the mixture less rich in L-menthol was less than for the others (Fig. S3b). Furthermore, the trend of $C_{p,m}$ with the composition was different because the trend of the molar mass with x_{Men} is opposite for both systems. Taherzadeh et al. [71] proposed a simple method to estimate the $C_{p,m}$ of the DESs at each temperature from the molar mass and the critical pressure of the mixtures. The equations are summarized in the Supplementary Material. With this procedure, we calculated $C_{p,m}$ for the mixtures studied here, and we compared the experimental and estimated results. The average deviations were $\overline{MRD}(C_{p,m}) = 3.8$ and 10% for [Men:Oct] and [Men:Dec], respectively. These values allow us to validate the correlation for this type of system, considering that the average deviation obtained by the authors was 4.7%.

In the same way as for the SLE, we also obtained the values of the three previous properties with PC-SAFT EoS in its predictive version and compared them with the values determined experimentally. For each mixture, the mean relative deviations are listed in Table S8. The model slightly overpredicted the density of both systems, and the deviations increased with the acid molar ratio (Fig. S4a). The average values were $\overline{MRD}(\rho) = 0.81\%$ for the system with Oct and $\overline{MRD}(\rho) = 0.77\%$ for the system with Dec. As usual, the deviations obtained for the speed of sound and for the isobaric molar heat capacity were greater since both properties were calculated as second-order derivatives [15]. For u, no clear trends with the temperature and composition were observed (Fig. S4b). For $C_{p,m}$, the deviations increased with the acid molar ratio (Fig. S4c). The average values were $\overline{MRD}(u) = 5.1\%$ and $\overline{MRD}(C_{p,m}) = 23\%$ for [Men:Oct] and $\overline{MRD}(u) = 9.3\%$ and $\overline{MRD}(C_{p,m}) = 5.6\%$ for [Men:Dec]. The validation of this EoS allows us its use to predict the volatility of the studied mixtures. The vapor pressure data at 298.15 K are listed in Table 2 and were less of 10 Pa, value that characterizes to the volatile organic compounds.

The value of the speed of light transmission through the materials is a function of their packing degree. Thus, the refractive index must be in agreement with the above observed trends of the compressibility. The less compact the fluid is, the lower the n_D data. Indeed, n_D was higher for the system with Dec and increased as x_{Men} and T decreased (Table 4, Fig. S3c). Our data matched the data from the literature [25] (Fig. S2c), and the $\overline{MRD}(n_D)$ was less than 0.01%. The molar refraction (R_m) is a measure of the hard core volume of a mole of molecules [72] and is calculated from ρ and n_D, with the Lorentz-Lorentz relationship:

$$R_m = \frac{M(n_D^2 - 1)}{\rho(n_D^2 + 2)}, \tag{2}$$

where M is the molar mass of the mixture (Table 2). For the [Men:Oct] system, the R_m values were 10% lower than the values for [Men:Dec], and contrary to the latter, they increased with the L-menthol molar ratio (Table 4). All data hardly changed with the

temperature (Fig. 6c). We estimated the percentage free volume by subtracting the molar volume from the molar refraction. The average value was 73.6%.

The permittivity is related to the structure of the polar fluids. According to the Kirkwood-Fröhlich model [73], the deviation from the randomness of the neighbouring dipoles can be estimated from the experimental data of macroscopic properties as ρ, n_D, and ε. Therefore, the Kirkwood parameter (g) was defined as:

$$g\mu^2 = \frac{9k_BT\varepsilon_0 M}{N_A\rho}\frac{\left(\varepsilon - n_D^2\right)\left(2\varepsilon + n_D^2\right)}{\varepsilon\left(n_D^2+2\right)^2}, \quad (3)$$

where ε_0, k_B and N_A are the vacuum static permittivity, the Boltzmann constant, and the Avogadro number, respectively. The dipole moment of the solution (μ) can be calculated from the values of the pure compounds (μ_i) as $\mu^2 = x_1\mu_1^2 + x_2\mu_2^2$. The g values greater than unity indicate that the fluid has adjacent dipoles preferably oriented in parallel. Conversely, the liquid with antiparallel orientation has the factor g < 1. Using the μ_{Men} and μ_{Oct} literature data (Table 1), the g values calculated for the [Men:Oct] system ranged from 0.81 to 1.26. A dipole parallel disposal was found for the least concentrated mixture, and the antiparallel dipoles increased with x_{Men}. This discussion is not available for the mixtures with Dec because no μ_{Dec} was found. Therefore, the polarization was analysed in terms of the orientational dipolar parameter ($\mu_{eff}^2 = g\mu^2$). Table 4 lists the values calculated for all mixtures at 298.15 K, and Fig. 6d shows the effects of the composition and temperature. Regarding the first variable, the mixtures with Oct were more polar, and the polarity increased with x_{Men}. In relation to T, a similar evolution of ε and μ_{eff}^2 would be expected, but opposite trends were obtained. ε decreased (Fig. S3d), and μ_{eff}^2 increased as T increased. This fact was already observed for [Thy]ESs [15] and other compounds [74], and it is explained considering that thermal agitation induces the breaking of cyclic aggregates; therefore, the number of linear aggregates with a higher effective dipole moment rises. The L-menthol-rich mixtures exhibited a slight minimum at 315 K.

Surface tension is an important property in processes whose effectiveness depends on the atomization of the fluid. The lower the values are, the greater the droplet formation capacity and more easily the fluid penetrates into tight spaces. Considering the experimental uncertainty, $U_c(\gamma)$, the measured data matched for all [Men:Oct] mixtures. For the other system, the values were slightly greater, and the lower the L-menthol molar ratio was, the more structured the liquid. At higher temperatures, a greater number of molecules have sufficient energy to move from the inside to the air-liquid interface, and the interactions are weaker so that γ decreases with increasing T (Fig. 5b). The linear variation was similar for all mixtures, so we can give an average value for the entropy of the surface per unit surface area, $\Delta S_S = -(\partial\gamma/\partial T)_p$= 0.076 ± 0.002 mN·m^{-1}·K^{-1}. The values of the enthalpy of the surface per unit surface area ($\Delta H_S = \gamma + T\Delta S_S$), barely changed with the composition for the [Men:Oct] system and decreased for the [Men:Dec] (Table 4). Although the data published by Nunes et al. [45] for other properties of the similar [Men:Oct] mixtures coincided with ours, their surface tension values were much lower (Fig. S2d). The average calculated deviation was $\overline{MRD}(\gamma)$ = 22.4%. Surface tension values allow us to estimate the critical temperature (T_c) of the fluids whose experimental determination is not possible because of the thermal degradation of the components. Thus, we estimated the T_c of our solvents (Table S11) with the Guggenheim [75] and Eötvos [76] expression (Supplementary Material) and predicted the critical loci with the PC-SAFT EoS (Fig. S5). To validate the results, we can compare the calculated T_c of pure Men, Oct, and Dec with values from the literature. The predicted values with the EoS agreed with those, and the deviations were less than 2 K. For both correlations, the results were similar, and the mean relative deviations were less than 1.5%. Considering that the PC-SAFT EoS provided a good representation of the phase behaviour and T_c of pure compounds, we can assume that the values obtained for [Men]ESs with this model were the most accurate. Compared with them, the deviations of the calculated data with the Guggenheim and Eötvos equations were 1.9 and 8.5%, respectively.

The viscosity of the liquids used as solvents is an operational parameter to consider in the design of industrial procedures because high fluidity increases their effectiveness. Contrary to most hydrophilic ESs or ionic liquids, hydrophobic eutectic mixtures have low or moderate η values, making them good candidates for mass transfer processes such as liquid-liquid or solid-liquid extraction, especially when phase separation is involved. van Osch et al. [47] have suggested 100 mPa·s as the maximum viscosity value for correct engineering processes. In this study, the measured η values were within 2.495–45.909 mPa·s, so they satisfied the above criteria. They were in agreement with those published by Nunes et al. [45] and Sas et al. [25] with average deviations of $\overline{MRD}(\eta)$ = 2.23 and 2.43%, respectively. However, our data were 9.85% higher than the data of Gonzalez et al. [39] and 22% lower than van Osch et al. [47] data (Fig. S2e). The longer chain in decanoic acid resulted in more viscous mixtures. In both systems, increasing the mole fraction of L-menthol dramatically increased the viscosity because the intermolecular interactions increased. However, η decreased with increasing T (Fig. 7a), especially at low temperatures, following the VFT equation (Table 5). The pre-exponential factor ($A_\eta = \eta_\infty$) is related to the contribution to the viscosity due only to steric effects. The other two parameters (B_Y and C_Y) allow the calculation of the energetic barrier to be overcome by the molecules to penetrate between the layers of the fluid, i.e., the energy of the viscous flow ($E_{a,\eta}$). The stronger the interactions, the highest $E_{a,\eta}$. Therefore, a polynomial decrease $E_{a,\eta} - T$ was observed (Fig. 7b). Comparing the equimolar mixtures, A_η was slightly higher for [Men:Dec], and the $E_{a,\eta}$ values were greater for this system (Table 4). At 298.15 K, the average difference was approximately 1.5 kJ·mol^{-1}. Pelofsky and Murkerjee equations provided two $\eta - \gamma$ correlations, which are reported in the Supplementary Material. Table S12 lists the regression coefficients, and Fig. S6 shows the logarithmic representation. The mean deviations between the experimental and calculated surface tensions were lower with the Murkerjee equation. The values for both correlations were $\overline{MRD}(\gamma)$ = 0.70 and 0.51% for mixtures with Oct and $\overline{MRD}(\gamma)$ = 0.47 and 0.37% for mixtures with Dec.

In summary, the increase in the length of the carboxylic acid chain decreased the compactness and polarity of the eutectic solvent but increased the surface tension and viscosity. The first effect can be beneficial to solubilize bulky compounds, but the others three, especially the last one, impair mass transfer processes. Finally, we compared the results of the thermophysical study of [Men]ESs with our previous paper on the characterization of similar mixtures with thymol [15]. Therefore, the effect of the aromatic ring can be evaluated. In this work, the ρ, u, n_D, α_p and γ values were lower and $\kappa_S, C_{p,m}$ and L_f were higher. In addition, the μ_{eff}, η, and $E_{a,\eta}$ were also larger. These results indicated that the [Men]ESs were both less compact and structured mixtures. However, the [Men]ESs were more polar and showed stronger intermolecular interactions. In thymol, the flatter structure of the aromatic ring allowed a higher compaction. Furthermore, the hydroxyl group donates electronic density into the conjugated π-ring via a resonance effect that is stronger than the inductive effect. As a consequence, the capacity to form hydrogen bonds with carboxylic acids could be reduced.

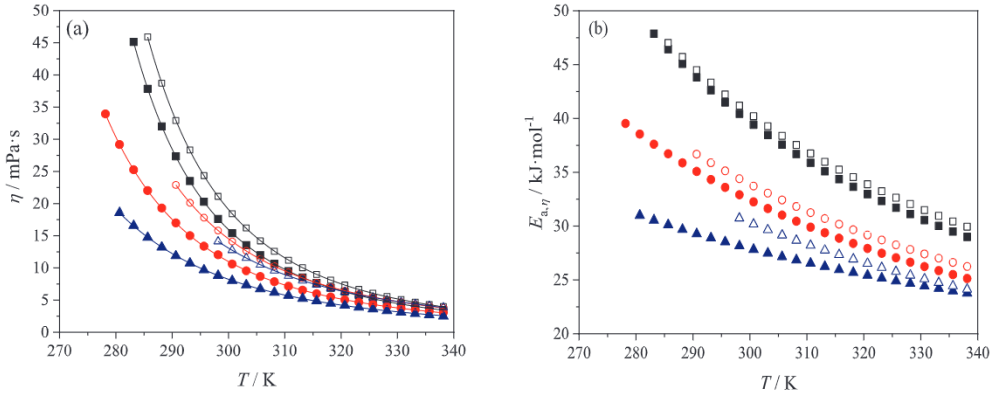

Fig. 7. Experimental and calculated transport properties of [Men]ESs at several temperatures, T, and compositions: (▲), (1:2); (●), (1:1); (■), (2:1) in molar ratio. (a), Dynamic viscosity, η; (b) energy of the viscous flow, $E_{a,\eta}$. Full symbols, [Men:Oct] system; empty symbols, [Men:Dec] system.

3.3. Solubility and extraction efficiency

The solubility of active principles (APIs) in water is probably the main problem in pharmacology. For a drug to be absorbed, it must be present as a solution at the site of absorption. Water is the solvent of choice for liquid formulations, but most APIs have low solubility, which implies low bioavailability and high toxicity in the gastrointestinal mucosa. However, some highly soluble compounds have poor metabolism, so enhanced hydrophobicity is adequate [77]. Different techniques have been developed to improve these parameters: (i) physical modifications such as reduction of the particle size, modification of the crystalline habit and dispersion of drugs in vehicles as eutectic mixtures or solid dispersions; (ii) chemical modifications such as pH change, buffer use, derivatization, complexation, and salt formation; and (iii) various methods including the use of adjuvants as surfactants, solubilizes, and new excipients [11,13–15,78].

In this section, we evaluated the solubility (W_i) of three poorly water-soluble compounds in the [Men]ESs characterized above. The chosen APIs were quercetin (Q), nitrofurantoin (NF), and tetracycline (TC). The first two substances belong to class II (low solubility and high permeability), and the third substance is a class III (high solubility and low permeability) substance according to the biopharmaceutical classification [77,79,80]. The solubility data of the APIs in the [Men]ESs are listed in Table 6. Q, NF, and TC were slightly soluble, insoluble and soluble, respectively, according to the pharmacopeia classification [81]. For Q, the solubility increased with increasing L-menthol concentration and, in general, was higher in the system with Dec. W_{NF} was very low in both systems but slightly higher in the mixtures with Dec. In this case, W_{NF} was lower at higher x_{Men}. Finally, W_{TC} was the highest and decreased as the acidity of the medium decreased. The solubility of a solute in a solvent is given by the intensity of the interaction among them. In our systems, these interactions can occur by hydrogen bonding and dipole-dipole forces. In relation to the first sites, Q has 5 donor and 7 acceptor sites, NF has 1 donor and 6 acceptor and TC has 6 donor and 9 acceptor sites (Fig. 1). Then, the affinity with the solvent due to this type of interaction follows the sequence TC > Q > NF. For the second ones, the polarizability of these molecules follows the same order, whereas NF has a higher dipole moment than Q (Table 1). The above results indicate the importance of the hydrogen bond network in the solubilization process of these APIs. Fig. 8 shows the ratio between the solubility measured in this work and the solubility in an aqueous medium [15]. Q presented the most pronounced increase, which was 100-fold greater than the increase for TC. Conversely, the use of these mixtures is not a suitable strategy to increase the solubility of NF. From our previous work [15], we can compare the solubility of these APIs in similar eutectic mixtures containing Men or Thy. The only structural difference between both compounds is the presence of the aromatic ring in Thy, which implies that it can establish π-stacking interactions but that it has a lower capacity to form hydrogen bonds by increasing its acidic character. Additionally, [Men]ES mixtures had higher effective dipole moments than [Thy]ESs. In this work, W_Q was 10-fold higher than in [Thy]ESs, so we can say that in this case, the hydrogen bonding interaction prevailed over the π-interaction. However, W_{NF} and W_{TC} in [Men]ESs were 10- and 2-fold lower, respectively, so the absence of the aromatic ring had a pronounced effect. Note that TC is a compound very affected by the pH of the medium, so for this API, the results should be more complex to analyse.

Table 6
Solubility ($W_i = g_i/g_{solvent}$) at T = 298.15 K, of quercetin (Q), nitrofurantoin (NF), and tetracycline (TC) in the studied [Men]ESs.

[Men]ESs	W_Q	W_{NF}	W_{TC}
[Men:Oct] (1:2)	$(1.83 \pm 0.09)\cdot10^{-3}$	$(6.16 \pm 0.23)\cdot10^{-5}$	0.113 ± 0.008
[Men:Oct] (1:1)	$(2.93 \pm 0.11)\cdot10^{-3}$	$(4.14 \pm 0.17)\cdot10^{-5}$	0.053 ± 0.003
[Men:Oct] (2:1)	$(4.55 \pm 0.17)\cdot10^{-3}$	$(3.84 \pm 0.12)\cdot10^{-5}$	0.039 ± 0.001
[Men:Dec] (1:2)	$(2.35 \pm 0.03)\cdot10^{-3}$	$(5.34 \pm 0.06)\cdot10^{-5}$	0.061 ± 0.004
[Men:Dec] (1:1)	$(3.74 \pm 0.23)\cdot10^{-3}$	$(3.33 \pm 0.22)\cdot10^{-5}$	0.066 ± 0.007
[Men:Dec] (2:1)	$(2.51 \pm 0.09)\cdot10^{-3}$	$(4.86 \pm 0.38)\cdot10^{-5}$	0.033 ± 0.003

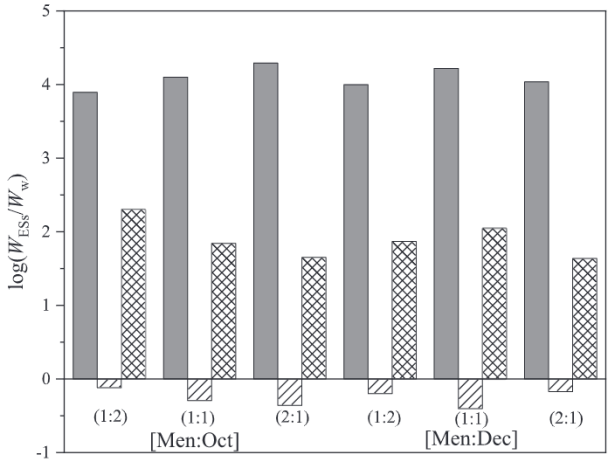

Fig. 8. Ratio between the solubility of several drugs in the eutectic mixtures and in water.

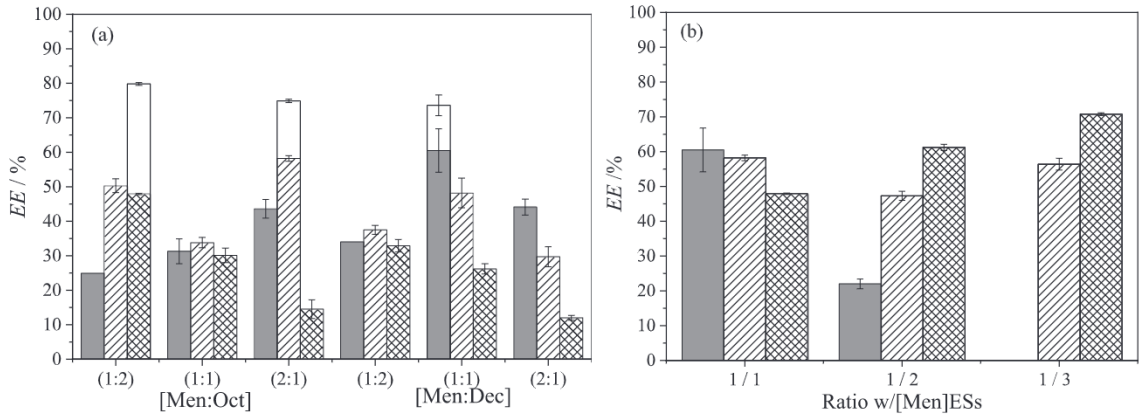

Fig. 9. Extraction efficiency, *EE*/%, of the [Men]ESs to remove drugs from water at*T* = 298.15 K. (a) 1 cycle: (▬), Q; (▨), NF; and (▩), TC; 3 cycles: (▭). (b) *EE* at several aqueous/organic ratios: (▬), Q+[Men:Dec] (1:1); (▨), NF+[Men:Oct] (2:1); and (▩), TC+[Men:Oct] (1:2).

Hydrophobic solvents can be used to remove substances from aqueous media. The literature reports studies about the removal of palladium, pesticides, phenolics, alcohols, phytocannabinoids, and pharmaceuticals [29,31–33,82] from contaminated water using [Men]ESs. Additionally, Sereshti et al. [83] eliminated TC from samples of contaminated milk. We evaluated the ability of [Men:Oct] and [Men:Dec] mixtures to remove Q, NF and TC from diluted aqueous solutions of these drugs. The working temperature was 298.15 K. Table S13 and Fig. 9a report the extraction efficiency (*EE*) obtained following the procedure described in the experimental section. The higher uncertainty of the quercetin results is related to its low initial concentration. For Q and TC, the trends were in agreement with the trends of the solubility; the *EE*(Q) of the mixtures with Oct increased as the L-menthol ratio and *EE*(TC) decreased. *EE*(TC) decreased to increase x_{Men} in the [Men:Dec] system, but the trend of *EE*(Q) and *EE*(NF) with the composition did not vary monotonically. The measured values were similar to the values reported in the aforementioned bibliography and much lower than the values found by us in the study with [Thy] ESs, explained by the lower affinity between the studied drugs and the mixtures with L-menthol as well as the lower density and higher viscosity of the mixtures with L-menthol. The effect of viscosity was more pronounced for the bulkier drug. In addition, it is important to highlight the effect of the presence of new water-ESs interactions as well as the interface. Abbas et al. [84] have shown that water causes strong changes in both the polarity and the number of hydrogen bonds in hydrophobic eutectic solvents. The authors concluded that the heterogeneity in the medium can hinder the extraction processes due to the accumulation of solutes in the interface. The partition coefficient values calculated (Table S13) for each drug and mixture, $P_{[Men]ESs/w}$, were lower than expected considering the solubility in water and in [Men]ESs and they varied with the x_{Men} . These results would be in agreement with the work of Abbas.

We have proved the chemical stability of all mixtures before and after the extraction process by NMR spectroscopy. The analysis of the organic phase showed that the signals were similar, to except a slight increase and displacement of the mobile hydroxyls (Fig. S7-S9). This fact is related to the dissolution of a small portion of water in [Men]ESs. In addition, the presence of low quantity of eutectic in the water was observed in the aqueous phase spectra (Fig S10).

Using the most efficient solvent for each drug, we performed a multistage extraction and determined the efficiency extraction at three aqueous/organic phase ratios. For all solutes, the *EE* increased with a three cycles process (Fig. 9a). The values were *EE*(Q) = 71%, *EE*(NF) = 75% and *EE*(TC) = 81%. On the other hand, the influence of the ratio was different depending on the solute. The *EE*(Q) decreased drastically as the organic phase increased until it was not detected at 1/3 ratio, the variation was not clear for NF, and *EE*(TC) increased (Fig. 9b). These values and the low toxicity of the solvent compared to the toxicity of drugs could justify its use for wastewater treatment of small hospital facilities or pharmaceutical industries.

4. Conclusions

This work extends the knowledge of the physicochemical behaviour of hydrophobic eutectic mixtures as well as their solvent capacity. Specifically, the mixtures contained L-menthol and octanoic or decanoic acid. To extend the knowledge, we begin by studying the solid-liquid phase diagram of both systems. The L-menthol polymorphism increased the complexity of this analysis. Multiple eutectic peaks favoured by the presence of the acid were obtained in the thermograms. Deconvolutions were necessary to calculate the eutectic composition. Both systems exhibited a slight negative deviation from ideality. Second, we measured seven thermophysical properties over a temperature range up to 338.15 K and at p = 1 bar. From the results, good separation in liquid-liquid extractions and adequate penetration of these solvents into the matrices can be expected because the density values were sufficiently lower than the density value of water, the surface tension was low and the viscosity was moderate. The refraction index and static permittivity allowed us to evaluate the polarizability of the fluids. In addition, we validated several correlations and thermodynamic models since predicting the behaviour of systems is highly desirable in the industry. Finally, the solubility of quercetin, nitrofurantoin and tetracycline in [Men]ESs was determined. For Q and TC, the solubility was drastically increased with respect to their solubility in water. Conversely, NF was slightly less soluble. Several ESs showed extraction efficiencies very different for the different drugs and lower than the extraction efficiencies previously published for eutectics with thymol. The absence of the aromatic ring and higher viscosity could be the explanation. An extraction process with 3 cycles allowed us to obtain efficiencies close to 80% for each drug.

In our opinion, this work can contribute the development of a database of thermophysical properties of fluids with the aim implementing new ecofriendly solvents in the industry. This issue is an important outlook within the field of green chemistry.

CRediT authorship contribution statement

Fernando Bergua: Investigation, Formal analysis. **Miguel Castro:** Investigation, Methodology. **José Muñoz-Embid:** Resources, Data curation. **Carlos Lafuente:** Validation, Writing – original draft, Funding acquisition. **Manuela Artal:** Project administration, Writing – original draft, Writing – review & editing.

Declaration of Competing Interest

The authors declare that they have no known competing financial interests or personal relationships that could have appeared to influence the work reported in this paper.

Acknowledgements

The PLATON research group acknowledges financial support from Gobierno de Aragón and Fondo Social Europeo "Construyendo Europa desde Aragón" E31_20R as well as from the University of Zaragoza (UZ2020-CIE-02).

Appendix A. Supplementary material

Supplementary data to this article can be found online at https://doi.org/10.1016/j.molliq.2022.118754.

References

[1] Petrochemical Group European, Solvents, 2021. www.petrochemistry.eu/sector-group/solvents/.
[2] Global market insights, 2021. www.gminsights.com/industry-analysis/organic-solvents-market.
[3] F.P. Byrne, S. Jin, G. Paggiola, T.H.M. Petchey, J.H. Clark, T.J. Farmer, A.J. Hunt, C. Robert McElroy, J. Sherwood, Tools and techniques for solvent selection: green solvent selection guides, Sustain. Chem. Process. 4 (2016) 1–24, https://doi.org/10.1186/s40508-016-0051-z.
[4] P. Harten, T. Martin, M. Gonzalez, D. Young, The software tool to find greener solvent replacements, PARIS III, Environ. Prog. Sustain Energy 39 (1) (2020) 13331, https://doi.org/10.1002/ep.13331.
[5] H. Sels, H. De Smet, J. Geuens, SUSSOL-Using artificial intelligence for greener solvent selection and substitution, Molecules 25 (2020) 1–26, https://doi.org/10.3390/molecules25133037.
[6] C.J. Clarke, W.-C. Tu, O. Levers, A. Bröhl, J.P. Hallett, Green and Sustainable Solvents in Chemical Processes, Chem. Rev. 118 (2) (2018) 747–800, https://doi.org/10.1021/acs.chemrev.7b00571.
[7] D.O. Abranches, M.A.R. Martins, L.P. Silva, N. Schaeffer, S.P. Pinho, J.A.P. Coutinho, Phenolic hydrogen bond donors in the formation of non-ionic deep eutectic solvents: The quest for type v des, Chem. Commun. 55 (69) (2019) 10253–10256.
[8] Y.H. Choi, J. van Spronsen, Y. Dai, M. Verberne, F. Hollmann, I.W.C.E. Arends, G.-J. Witkamp, R. Verpoorte, Are Natural Deep Eutectic Solvents the Missing Link in Understanding Cellular Metabolism and Physiology?, Plant Physiol 156 (2011) 1701–1705, https://doi.org/10.1104/pp.111.178426.
[9] A. Mišan, J. Nađpal, A. Stupar, M. Pojić, A. Mandić, R. Verpoorte, Y.H. Choi, The perspectives of natural deep eutectic solvents in agri-food sector, Crit. Rev. Food Sci. Nutr. 60 (15) (2020) 2564–2592, https://doi.org/10.1080/10408398.2019.1650717.
[10] W. Tang, Y. An, K.H. Row, Emerging applications of (micro) extraction phase from hydrophilic to hydrophobic deep eutectic solvents: opportunities and trends, TrAC Trends Anal. Chem. 136 (2021) 116187, https://doi.org/10.1016/j.trac.2021.116187.
[11] J. Haneef, S. Ali, R. Chadha, Emerging Multi-Drug Eutectics: Opportunities and Challenges, AAPS PharmSciTech. 22 (2021) 66, https://doi.org/10.1208/s12249-021-01939-6.
[12] G.C. Bazzo, B.R. Pezzini, H.K. Stulzer, Eutectic mixtures as an approach to enhance solubility, dissolution rate and oral bioavailability of poorly water-soluble drugs, Int. J. Pharm. 588 (2020) 119741, https://doi.org/10.1016/j.ijpharm.2020.119741.
[13] N. López, I. Delso, D. Matute, C. Lafuente, M. Artal, Characterization of xylitol or citric acid:choline chloride:water mixtures: Structure, thermophysical properties, and quercetin solubility, Food Chem. 306 (2020) 125610, https://doi.org/10.1016/j.foodchem.2019.125610.
[14] F. Bergua, I. Delso, J. Muñoz-Embid, C. Lafuente, M. Artal, Structure and properties of two glucose-based deep eutectic systems, Food Chem. 336 (2021) 127717, https://doi.org/10.1016/j.foodchem.2020.127717.
[15] F. Bergua, M. Castro, J. Muñoz-Embid, C. Lafuente, M. Artal, Hydrophobic eutectic solvents: Thermophysical study and application in removal of pharmaceutical products from water, Chem. Eng. J. 411 (2021) 128472, https://doi.org/10.1016/j.cej.2021.128472.
[16] C. Florindo, L.C. Branco, I.M. Marrucho, Quest for Green-Solvent Design: From Hydrophilic to Hydrophobic (Deep) Eutectic Solvents, ChemSusChem. 12 (8) (2019) 1549–1559, https://doi.org/10.1002/cssc.201900147.
[17] D.J.G.P. van Osch, L.F. Zubeir, A. van den Bruinhorst, M.A.A. Rocha, M.C. Kroon, Hydrophobic deep eutectic solvents as water-immiscible extractants, Green Chem. 17 (9) (2015) 4518–4521.
[18] D.J.G.P. Van Osch, C.H.J.T. Dietz, S.E.E. Warrag, M.C. Kroon, The Curious Case of Hydrophobic Deep Eutectic Solvents: A Story on the Discovery, Design, and Applications, ACS Sustain. Chem. Eng. 8 (2020) 10591–10612, https://doi.org/10.1021/acssuschemeng.0c00559.
[19] T. Lemaoui, A.S. Darwish, A. Attoui, F. Abu Hatab, N.E.H. Hammoudi, Y. Benguerba, L.F. Vega, I.M. Alnashef, Predicting the density and viscosity of hydrophobic eutectic solvents: Towards the development of sustainable solvents, Green Chem. 22 (23) (2020) 8511–8530.
[20] J.M. Edgecomb, E.E. Tereshatov, G. Zante, M. Boltoeva, C.M. Folden III, Hydrophobic amine-based binary mixtures of active pharmaceutical and food grade ingredients: Characterization and application in indium extraction from aqueous hydrochloric acid media, Green Chem. 22 (20) (2020) 7047–7058.
[21] UNESCO, WWAP (United Nations World Water Assessment Programme), The United Nations World Water Development Report 2018: Nature-based Solutions. Paris, UNESCO, 2018.
[22] M. Patel, R. Kumar, K. Kishor, T. Mlsna, C.U. Pittman, D. Mohan, Pharmaceuticals of emerging concern in aquatic systems: Chemistry, occurrence, effects, and removal methods, Chem. Rev. 119 (6) (2019) 3510–3673, https://doi.org/10.1021/acs.chemrev.8b00299.
[23] S. Rodriguez-Mozaz, I. Vaz-Moreira, S. Varela Della Giustina, M. Llorca, D. Barceló, S. Schubert, T.U. Berendonk, I. Michael-Kordatou, D. Fatta-Kassinos, J. L. Martinez, C. Elpers, I. Henriques, T. Jaeger, T. Schwartz, E. Paulshus, K. O'Sullivan, K.M.M. Pärnänen, M. Virta, T.T. Do, F. Walsh, C.M. Manaia, Antibiotic residues in final effluents of European wastewater treatment plants and their impact on the aquatic environment, Environ. Int. 140 (2020) 105733, https://doi.org/10.1016/j.envint.2020.105733.
[24] J. Wang, S. Wang, Removal of pharmaceuticals and personal care products (PPCPs) from wastewater: A review, J. Environ. Manage. 182 (2016) 620–640, https://doi.org/10.1016/j.jenvman.2016.07.049.
[25] O.G. Sas, M. Castro, Á. Domínguez, B. González, Removing phenolic pollutants using Deep Eutectic Solvents, Sep. Purif. Technol. 227 (2019) 115703, https://doi.org/10.1016/j.seppur.2019.115703.
[26] G. Almustafa, R. Sulaiman, M. Kumar, I. Adeyemi, H.A. Arafat, I. AlNashef, Boron extraction from aqueous medium using novel hydrophobic deep eutectic solvents, Chem. Eng. J. 395 (2020) 125173, https://doi.org/10.1016/j.cej.2020.125173.
[27] P. Makoś, E. Słupek, J. Gębicki, Hydrophobic deep eutectic solvents in microextraction techniques–A review, Microchem. J. 152 (2020) 104384, https://doi.org/10.1016/j.microc.2019.104384.
[28] K.e. Li, Y. Jin, D. Jung, K. Park, H. Kim, J. Lee, In situ formation of thymol-based hydrophobic deep eutectic solvents: Application to antibiotics analysis in surface water based on liquid-liquid microextraction followed by liquid chromatography, J. Chromatogr. A 1614 (2020) 460730, https://doi.org/10.1016/j.chroma.2019.460730.
[29] K. Abdi, M. Ezoddin, N. Pirooznia, Temperature-controlled liquid–liquid microextraction using a biocompatible hydrophobic deep eutectic solvent for microextraction of palladium from catalytic converter and road dust samples prior to ETAAS determination, Microchem. J. 157 (2020) 104999, https://doi.org/10.1016/j.microc.2020.104999.
[30] R. Verma, T. Banerjee, Liquid-Liquid Extraction of Lower Alcohols Using Menthol-Based Hydrophobic Deep Eutectic Solvent: Experiments and COSMO-SAC Predictions, Ind. Eng. Chem. Res. 57 (9) (2018) 3371–3381, https://doi.org/10.1021/acs.iecr.7b0527010.1021/acs.iecr.7b05270.s001.
[31] T. Křížek, M. Bursová, R. Horsley, M. Kuchař, P. Tůma, R. Čabala, T. Hložek, Menthol-based hydrophobic deep eutectic solvents: Towards greener and efficient extraction of phytocannabinoids, J. Clean. Prod. 193 (2018) 391–396, https://doi.org/10.1016/j.jclepro.2018.05.080.
[32] C. Florindo, L.C.C. Branco, I.M.M. Marrucho, Development of hydrophobic deep eutectic solvents for extraction of pesticides from aqueous environments, Fluid Phase Equilib. 448 (2017) 135–142, https://doi.org/10.1016/j.fluid.2017.04.002.
[33] R. Cañadas, M. González-Miquel, E.J. González, I. Díaz, M. Rodríguez, Hydrophobic eutectic solvents for extraction of natural phenolic antioxidants from winery wastewater, Sep. Purif. Technol. 254 (2021) 117590, https://doi.org/10.1016/j.seppur.2020.117590.
[34] C. Florindo, F. Lima, L.C. Branco, I.M. Marrucho, Hydrophobic Deep Eutectic Solvents: A Circular Approach to Purify Water Contaminated with Ciprofloxacin, ACS Sustain. Chem. Eng. 7 (17) (2019) 14739–14746, https://doi.org/10.1021/acssuschemeng.9b02658.
[35] N. Schaeffer, J.H.F. Conceição, M.A.R. Martins, M.C. Neves, G. Pérez-Sánchez, J.R. B. Gomes, N. Papaiconomou, J.A.P. Coutinho, Non-ionic hydrophobic eutectics-versatile solvents for tailored metal separation and valorisation, Green Chem. 22 (9) (2020) 2810–2820.
[36] D. Rodríguez-Llorente, P. Navarro, R. Santiago, V.I. Águeda, S. Álvarez-Torrellas, J. García, M. Larriba, Extractive removal and recovery of bisphenol A from aqueous solutions using terpenoids and hydrophobic eutectic solvents, J. Environ. Chem. Eng. 9 (5) (2021) 106128.

[37] M. Kurjogi, Y.H. Issa Mohammad, S. Alghamdi, M. Abdelrahman, P. Satapute, S. Jogaiah, Z. Zhou, Detection and determination of stability of the antibiotic residues in cow's milk, PLoS One. 14 (10) (2019) e0223475, https://doi.org/10.1371/journal.pone.0223475.
[38] D. Althans, P. Schrader, S. Enders, Solubilisation of quercetin: Comparison of hyperbranched polymer and hydrogel, J. Mol. Liq. 196 (2014) 86–93, https://doi.org/10.1016/j.molliq.2014.03.028.
[39] E.J. González, M. González-Miquel, I. Díaz, M. Rodríguez, C. Fontela, R. Cañadas, J. Sánchez, Enhancing aqueous systems fermentability using hydrophobic eutectic solvents as extractans of inhibitory compounds, Sep. Purif. Technol. 250 (2020) 117184, https://doi.org/10.1016/j.seppur.2020.117184.
[40] I. Adeyemi, R. Sulaiman, M. Almazroui, A. Al-Hammadi, I.M. AlNashef, Removal of chlorophenols from aqueous media with hydrophobic deep eutectic solvents: Experimental study and COSMO RS evaluation, J. Mol. Liq. 311 (2020) 113180, https://doi.org/10.1016/j.molliq.2020.113180.
[41] R. Hollenbach, K. Ochsenreither, C. Syldatk, Enzymatic synthesis of glucose monodecanoate in a hydrophobic deep eutectic solvent, Int. J. Mol. Sci. 21 (2020) 1–11, https://doi.org/10.3390/ijms21124342.
[42] A. Alhadid, L. Mokrushina, M. Minceva, Design of deep eutectic systems: A simple approach for preselecting eutectic mixture constituents, Molecules 25 (2020) 1–11, https://doi.org/10.3390/molecules25051077.
[43] J. Wen, Y. Lu, L. Shi, Y. Yang, A novel cloud point extraction based on fatty acid deep eutectic solvent combined with high-performance liquid chromatography for determination of ultraviolet absorbent in food packaging bags, Microchem. J. 153 (2020) 8–12, https://doi.org/10.1016/j.microc.2019.104466.
[44] H.H. Ali, M.M. Ghareeb, M. Al-Remawi, F.T. Al-Akayleh, New insight into sin7gle phase formation of capric acid/menthol eutectic mixtures by Fourier-transform infrared spectroscopy and differential scanning calorimetry, Trop. J. Pharm. Res. 19 (2020) 361–369, https://doi.org/10.4314/tjpr.v19i2.19.
[45] R.J. Nunes, B. Saramago, I.M. Marrucho, Surface Tension of dl -Menthol: Octanoic Acid Eutectic Mixtures, J. Chem. Eng. Data. 64 (2019) 4915–4923, https://doi.org/10.1021/acs.jced.9b00424.
[46] F. Al-Akayleh, H.H. Mohammed Ali, M.M. Ghareeb, M. Al-Remawi, Therapeutic deep eutectic system of capric acid and menthol: Characterization and pharmaceutical application, J. Drug Deliv Sci. Technol. 53 (2019) 101159, https://doi.org/10.1016/j.jddst.2019.101159.
[47] D.J.G.P. van Osch, C.H.J.T. Dietz, J. van Spronsen, M.C. Kroon, F. Gallucci, M. van Sint Annaland, R. Tuinier, A Search for Natural Hydrophobic Deep Eutectic Solvents Based on Natural Components, ACS Sustain. Chem. Eng. 7 (3) (2019) 2933–2942, https://doi.org/10.1021/acssuschemeng.8b0352010.1021/acssuschemeng.8b03520.s001.
[48] M. Nedaei, A.R. Zarei, S.A. Ghorbanian, Development of a new emulsification microextraction method based on solidification of settled organic drop: Application of a novel ultra-hydrophobic tailor-made deep eutectic solvent, New J. Chem. 42 (15) (2018) 12520–12529.
[49] M.A.R. Martins, E.A. Crespo, P.V.A. Pontes, L.P. Silva, M. Bülow, G.J. Maximo, E.A. C. Batista, C. Held, S.P. Pinho, J.A.P. Coutinho, Tunable Hydrophobic Eutectic Solvents Based on Terpenes and Monocarboxylic Acids, ACS Sustain. Chem. Eng. 6 (7) (2018) 8836–8846, https://doi.org/10.1021/acssuschemeng.8b0120310.1021/acssuschemeng.8b01203.s001.
[50] L. Percevault, A. Jani, T. Sohier, L. Noirez, L. Paquin, F. Gauffre, D. Morineau, Do Deep Eutectic Solvents Form Uniform Mixtures beyond Molecular Microheterogeneities?, J Phys. Chem. B 124 (41) (2020) 9126–9135, https://doi.org/10.1021/acs.jpcb.0c0631710.1021/acs.jpcb.0c06317.s001.
[51] N. Paul, P.K. Naik, B.D. Ribeiro, P.S. Gooh Pattader, I.M. Marrucho, T. Banerjee, Molecular dynamics insights and water stability of hydrophobic deep eutectic solvents aided extraction of nitenpyram from an aqueous environment, J. Phys. Chem. B 124 (34) (2020) 7405–7420, https://doi.org/10.1021/acs.jpcb.0c0364710.1021/acs.jpcb.0c03647.s001.
[52] R. Maruchenko, P. Espeau, Revised phase diagrams based on racemic ibuprofen with thymol and l-menthol, J. Therm. Anal. Calorim. 145 (6) (2021) 3087–3091, https://doi.org/10.1007/s10973-020-10119-w.
[53] Stenutz, (n.d.). http://www.stenutz.eu/chem/.
[54] Pubchem, (n.d.). https://pubchem.ncbi.nlm.nih.gov/.
[55] A.M. Mendoza-Wilson, D. Glossman-Mitnik, CHIH-DFT study of the electronic properties and chemical reactivity of quercetin, J. Mol. Struct. THEOCHEM. 716 (1-3) (2005) 67–72, https://doi.org/10.1016/j.theochem.2004.10.083.
[56] U. of A. A.M. Matuszek, Defining Known Drug Space by DFT based molecular descriptors. Virtual screening for novel Atg5-Atg16 complex inhibitors for autophagy modulation, 2014.
[57] V. Antón, H. Artigas, J. Muñoz-Embid, M. Artal, C. Lafuente, Thermophysical study of 2-acetylthiophene: Experimental and modelled results, Fluid Phase Equilib. 433 (2017) 126–134, https://doi.org/10.1016/j.fluid.2016.10.026.
[58] A. Alhadid, L. Mokrushina, M. Minceva, Formation of glassy phases and polymorphism in deep eutectic solvents, J. Mol. Liq. 314 (2020) 113667, https://doi.org/10.1016/j.molliq.2020.113667.
[59] V. Štejfa, A. Bazyleva, M. Fulem, J. Rohlíček, E. Skořepová, K. Růžička, A.V. Blokhin, Polymorphism and thermophysical properties of l- and dl-menthol, J. Chem. Thermodyn. 131 (2019) 524–543, https://doi.org/10.1016/j.jct.2018.11.004.
[60] Y. Corvis, P. Espeau, Incidence of chirality on the properties of mixtures containing an amide type anesthetic compound, Thermochim. Acta 539 (2012) 39–43, https://doi.org/10.1016/j.tca.2012.03.027.
[61] Y. Corvis, A. Wurm, C. Schick, P. Espeau, New menthol polymorphs identified by flash scanning calorimetry, CrystEngComm. 17 (29) (2015) 5357–5359, https://doi.org/10.1039/C5CE00697J.
[62] J. Bernstein, R.J. Davey, J.-O. Henck, Concomitant Polymorphs, Angew. Chem., Int. Ed. 38 (23) (1999) 3440–3461.
[63] Y. Corvis, P. Espeau, Interpretation of the global heat of melting in eutectic binary systems, Thermochim. Acta. 664 (2018) 91–99, https://doi.org/10.1016/j.tca.2018.04.011.
[64] L. Rycerz, Practical remarks concerning phase diagrams determination on the basis of differential scanning calorimetry measurements, J. Therm. Anal. Calorim. 113 (1) (2013) 231–238, https://doi.org/10.1007/s10973-013-3097-0.
[65] J.M. Silva, C.V. Pereira, F. Mano, E. Silva, V.I.B. Castro, I. Sá-Nogueira, R.L. Reis, A. Paiva, A.A. Matias, A.R.C. Duarte, Therapeutic Role of Deep Eutectic Solvents Based on Menthol and Saturated Fatty Acids on Wound Healing, ACS Appl. Bio Mater. 2 (10) (2019) 4346–4355, https://doi.org/10.1021/acsabm.9b00598.
[66] H. Renon, J.M. Prausnitz, Local compositions in thermodynamic excess functions for liquid mixtures, AIChE J. 14 (1) (1968) 135–144, https://doi.org/10.1002/aic.690140124.
[67] E.G. Prausnitz, J.M. Lichtenthaler, R.N. Azevedo, Molecular Thermodynamics of the Fluid Phase Equilibria, Prentice-Hall, 1986.
[68] J. Gross, G. Sadowski, Application of perturbation theory to a hard-chain reference fluid: An equation of state for square-well chains, Fluid Phase Equilib. 168 (2) (2000) 183–199, https://doi.org/10.1016/S0378-3812(00)00302-2.
[69] J. Gross, G. Sadowski, Perturbed-chain SAFT: An equation of state based on a perturbation theory for chain molecules, Ind. Eng. Chem. Res. 40 (2001) 1244–1260, https://doi.org/10.1021/ie0003887.
[70] B. Jacobson, Ultrasonic Velocity in Liquids and Liquid Mixtures, J. Chem. Phys. 20 (5) (1952) 927–928, https://doi.org/10.1063/1.1700615.
[71] M. Taherzadeh, R. Haghbakhsh, A.R.C. Duarte, S. Raeissi, Estimation of the heat capacities of deep eutectic solvents, J. Mol. Liq. 307 (2020) 112940, https://doi.org/10.1016/j.molliq.2020.112940.
[72] P. Brocos, Á. Piñeiro, R. Bravo, A. Amigo, Refractive indices, molar volumes and molar refractions of binary liquid mixtures: Concepts and correlations, Phys. Chem. Chem. Phys. 5 (2003) 550–557, https://doi.org/10.1039/b208765k.
[73] H. Fröhlich, General theory of the static dielectric constant, Trans. Faraday Soc. 44 (0) (1948) 238–243, https://doi.org/10.1039/TF9484400238.
[74] R. Bouteloup, D. Mathieu, Predicting dielectric constants of pure liquids: Fragment-based Kirkwood-Fröhlich model applicable over a wide range of polarity, Phys. Chem. Chem. Phys. 21 (21) (2019) 11043–11057.
[75] E.A. Guggenheim, The Principle of Corresponding States, J. Chem. Phys. 13 (7) (1945) 253–261, https://doi.org/10.1063/1.1724033.
[76] J.L. Shereshefsky, Surface tension of saturated vapors and the equation of Eötvos, J. Phys. Chem. 35 (1930) 1712–1720.
[77] J.M. Custodio, C.-Y. Wu, L.Z. Benet, Predicting drug disposition, absorption/elimination/transporter interplay and the role of food on drug absorption, Adv. Drug Deliv. Rev. 60 (6) (2008) 717–733, https://doi.org/10.1016/j.addr.2007.08.043.
[78] K.T. Savjani, A.K. Gajjar, J.K. Savjani, Drug Solubility: Importance and Enhancement Techniques, ISRN Pharm. 2012 (2012) 1–10, https://doi.org/10.5402/2012/195727.
[79] X.-Y. Teoh, F.N. bt Mahyuddin, W. Ahmad, S.-Y. Chan, Formulation strategy of nitrofurantoin: co-crystal or solid dispersion?, Pharm Dev. Technol. 25 (2) (2020) 245–251, https://doi.org/10.1080/10837450.2019.1689401.
[80] L. Rao, A Review on Quercetin: Assessment of the Pharmacological Potentials and Various Formulations Strategies, Int. J. Pharm. Sci. Rev. Res. 64 (2020) 139–144, https://doi.org/10.47583/ijpsrr.2020.v64i01.026.
[81] Pharmacopeia of the United States of America, 32nd revision, and the National Formulary, 27th edition, 2009.
[82] R. Verma, M. Mohan, V.V. Goud, T. Banerjee, Operational Strategies and Comprehensive Evaluation of Menthol Based Deep Eutectic Solvent for the Extraction of Lower Alcohols from Aqueous Media, ACS Sustain. Chem. Eng. 6 (12) (2018) 16920–16932, https://doi.org/10.1021/acssuschemeng.8b0425510.1021/acssuschemeng.8b04255.s001.
[83] H. Sereshti, S. Semnani Jazani, N. Nouri, G. Shams, Dispersive liquid–liquid microextraction based on hydrophobic deep eutectic solvents: Application for tetracyclines monitoring in milk, Microchem. J. 158 (2020) 105269, https://doi.org/10.1016/j.microc.2020.105269.
[84] U.L. Abbas, Q.i. Qiao, M.T. Nguyen, J. Shi, Q. Shao, Molecular dynamics simulations of heterogeneous hydrogen bond environment in hydrophobic deep eutectic solvents, AIChE J. 68 (1) (2022), https://doi.org/10.1002/aic.17382.